

Original citation:

Alonso-Orts, Manuel, Sanchez, Ana M., Hindmarsh, Steven, López, Iñaki , Nogales, Emilio , Piqueras, Javier and Méndez, Bianchi. (2017) Shape engineering driven by selective growth of SnO₂ on doped Ga₂O₃ nanowires. Nano Letters, 17 (1). pp. 515-522.

Permanent WRAP URL:

<http://wrap.warwick.ac.uk/86195>

Copyright and reuse:

The Warwick Research Archive Portal (WRAP) makes this work by researchers of the University of Warwick available open access under the following conditions. Copyright © and all moral rights to the version of the paper presented here belong to the individual author(s) and/or other copyright owners. To the extent reasonable and practicable the material made available in WRAP has been checked for eligibility before being made available.

Copies of full items can be used for personal research or study, educational, or not-for profit purposes without prior permission or charge. Provided that the authors, title and full bibliographic details are credited, a hyperlink and/or URL is given for the original metadata page and the content is not changed in any way.

Publisher's statement:

"This document is the Accepted Manuscript version of a Published Work that appeared in final form in Nano Letters. copyright © American Chemical Society after peer review and technical editing by the publisher.

To access the final edited and published work

<http://pubs.acs.org/page/policy/articlesonrequest/index.html> ."

A note on versions:

The version presented here may differ from the published version or, version of record, if you wish to cite this item you are advised to consult the publisher's version. Please see the 'permanent WRAP URL above for details on accessing the published version and note that access may require a subscription.

For more information, please contact the WRAP Team at: wrap@warwick.ac.uk

Shape engineering driven by selective growth of SnO₂ on doped Ga₂O₃ nanowires

Manuel Alonso-Orts[†], Ana M. Sánchez[‡], Steven A. Hindmarsh[‡], Iñaki López[†], Emilio Nogales[†], Javier Piqueras[†], Bianchi Méndez*^{†,‡}*

[†]Departamento de Física de Materiales, Facultad de Ciencias Físicas, Universidad Complutense de Madrid, 28040-Madrid, Spain

[‡]Department of Physics, University of Warwick, Coventry, CV4 7AL, United Kingdom

KEYWORDS. Complex oxide nanowires, selective growth, crossed nanowires, transmission electron microscopy, cathodoluminescence

ABSTRACT. Tailoring the shape of complex nanostructures requires control of the growth process. In this work, we report on the selective growth of nanostructured tin oxide on gallium oxide nanowires leading to the formation of SnO₂/Ga₂O₃ complex nanostructures. Ga₂O₃ nanowires decorated with either crossing SnO₂ nanowires or SnO₂ particles have been obtained in a single step treatment, by thermal evaporation. The reason for this dual behavior is related to the growth direction of trunk Ga₂O₃ nanowires. Ga₂O₃ nanowires grown along the [001] direction favor the formation of crossing SnO₂ nanowires. Alternatively, SnO₂ forms rhombohedral particles on [110] Ga₂O₃ nanowires leading to skewer-like structures. These complex oxide structures were

grown by a catalyst-free vapor-solid process. When pure Ga and tin oxide were used as source materials and compacted powders of Ga_2O_3 acted as substrates, $[110]$ Ga_2O_3 nanowires grow preferentially. High-resolution transmission electron microscopy analysis reveals epitaxial relationship lattice matching between the Ga_2O_3 axis and SnO_2 particles, forming skewer-like structures. The addition of chromium oxide to the source materials modifies the growth direction of the trunk Ga_2O_3 nanowires, growing along the $[001]$, with crossing SnO_2 wires. The $\text{SnO}_2/\text{Ga}_2\text{O}_3$ junctions does not meet the lattice matching condition, forming a grain boundary. The electronic and optical properties have been studied by XPS and CL with high spatial resolution, enabling us to get both local chemical and electronic information of the surface in both type of structures. The results will allow tuning optical and electronic properties of oxide complex nanostructures locally as a function of the orientation. In particular, we report a dependence of the visible CL emission of SnO_2 on its particular shape. Orange emission dominates in $\text{SnO}_2/\text{Ga}_2\text{O}_3$ crossing wires while green-blue emission is observed in SnO_2 particles attached to Ga_2O_3 trunks. The results show that the Ga_2O_3 - SnO_2 system appears to be a benchmark for shape engineering to get architectures involving nanowires via the control of the growth direction of the nanowires.

TEXT

Advances in smart nanostructured materials require a deep understanding of the growth mechanisms to develop novel designs and architectures. Engineering new architectures will enable the combination of zero-, one- and two-dimensional systems enhancing the functionalities in comparison with their single counterparts (quantum dots, nanowires or nanosheets)¹. Some physical properties, such as optical and transport properties, could be strongly dependent on the morphology of nanomaterials, hence nanomaterials with mixed dimensionality could offer extra

applications. For example, light emission in nanowires may be affected if nanowires are assembled with quantum dots in the same nanostructure². Beside dimensionality, we can even broaden out the tailoring capabilities of nanostructured materials by mixing several chemical elements or compounds. For instance, 1D-TiO₂/2D-ZnIn₂S₄ nanostructures with improved photocatalytic properties have been very recently reported³. Semiconducting oxides are an attractive family of smart materials with wide range of morphologies within the quasi-one dimension (nanowires, nanobelts, or nanorods)⁴. Besides, these oxides offer a high versatility in the applications: optical and mechanical resonators, lasing, sensors, photo-catalysis, solar cells, and biomedical and healthcare usages, to name a few⁵⁻⁸. A great deal of research has been focused on synthesis, characterization and applications of semiconducting oxide nanowires in the last decade, although there are still open questions. From the point of view of the physical properties, for example, it is still a challenge to get effectively doped oxide nanowires with controllable conductivity⁹. On the other hand, surface properties play a key role in the case of nanomaterials due to the high aspect ratio of nanowires and nanoparticles. The surface influences both the physical-chemical properties and the growth mechanisms to generate specific architectures. Here, there is still room for improvement. In the case of Si nanowires, a model based on Plateau-Rayleigh instability has been recently proposed to generate one-dimensional Si-Ge heterostructures with modulation in their diameter, in which surface energy considerations drive the growth and playing with the kinetical factors enable the shape-tailoring^{10,11}. Alternatively, in III-V nanowires surface energy engineering has been also exploited to control the polarity and the kink formation in III-V nanowires¹². Hence, gaining knowledge about the relationship between crystal orientation and final morphology will contribute to understand the formation of nano-oxide assemblies and to get further control over their final shape.

Even though many works on hierarchical or complex nanostructures have been reported, most of semiconducting oxide nanomaterials refer to objects with homogeneous chemical composition, obtained from several routes¹³⁻¹⁵. In previous works, we have successfully grown a large variety of low dimensional semiconducting oxide structures by thermal evaporation of chemical precursors under suitable thermal treatment parameters (gas flow and temperature). In particular, nanowires, nanotubes or nanorods of ZnO, SnO₂, GeO₂, Sb₂O₃, In₂O₃, Ga₂O₃ among others, with well-defined facets and high crystalline quality have already been reported¹⁶⁻¹⁹. In this work, we tackle the synthesis and characterization of some specific Ga₂O₃/SnO₂ architectures grown by a catalyst free vapor-solid (VS) mechanism. Monoclinic β -Ga₂O₃ and rutile SnO₂ are the thermodynamically stable phases of Ga₂O₃ and SnO₂, respectively. Their wide band gaps (4.9 eV and 3.7 eV, respectively) make them suitable for applications in the ultraviolet range. Their chemical stability, easiness of production and tune ability of physical properties make these oxides a potentially interesting alternative to other wide band gap semiconductors, such as the nitride family. Photodetectors and photocatalytic applications, as well as chemical sensors, batteries, light emitters, and energy applications have been anticipated using Ga₂O₃ or SnO₂ films and/or nanostructures²⁰⁻²³. In most of these applications, the surface plays a key role in the performance of the devices based on these oxides. The development of nanostructures combining these two oxides could be very promising from the point of view of applications. Ga₂O₃/SnO₂ heterostructures, which consisted of Sn-doped Ga₂O₃ and polycrystalline Ga-doped SnO₂ assembled in nanowires have been reported for sensing applications²⁴. Also, Hsu and Lu reported the fabrication of Ga₂O₃/SnO₂ core-shell nanostructures with applications in ultraviolet detectors²⁵. By using the above-mentioned VS catalyst free method, we have grown crossed Ga₂O₃/SnO₂ multiwire architecture and a detailed characterization of the heterojunctions has been

carried out²⁶. Here, we report the growth and characterization of two kinds of nano-heterostructures that have a main Ga₂O₃ nanowire axis: skewer-like (SK) structures with small SnO₂ particles attached to the trunk; and crossed wires (CW) structures consisting of SnO₂ wires cutting across a central Ga₂O₃ nanowire. The goal is to understand the underlying formation mechanisms and the main features of these heterostructures that could be extended to other oxide materials.

Single-step thermal treatments of metallic gallium along with tin oxide powders at 1500 °C for 15 hours were conducted under argon flow in order to get conditions for the growth of both Ga₂O₃ and SnO₂ nanostructures. Alternatively, a small fraction of chromium oxide was added to the precursors and the same thermal treatment was carried out. Sn or Cr impurities have **been** proved to increase the production yield of GeO₂ and Sb₂O₃ nanowires or nanorods during the thermal treatment, respectively²⁷⁻²⁸. It was previously found that addition of a small amount of tin oxide powders to the Ga source, branched Ga₂O₃ nanowires were developed during a 1350 °C thermal treatment. Sn impurities were segregated towards the surface of the main Ga₂O₃ trunks during the thermal growth and became nucleation sites for secondary Ga₂O₃ branches²⁹. In that case, the temperature was not enough to nucleate SnO₂ nanostructures. In the present work, the temperature has been increased up to 1500 °C. This temperature is closer to the melting point of SnO₂ and Ga₂O₃ (1630 °C and 1725 °C, respectively), which makes feasible the stabilization of both SnO₂ and Ga₂O₃ crystals.

In this work, two different heterostructures, skewer-like (Figure 1a) and crossed nanowires (Figure 1b) were analyzed in detail. Both are formed by a main longitudinal Ga₂O₃ nanowire with SnO₂ nanoparticles or transversal SnO₂ nanowire. The structure and morphology of these nanostructures were analyzed by high resolution (Scanning) Transmission Electron Microscopy

((S)TEM) using a JEOL 2100 and a double corrected ARM 200F microscopes working at 200kV. Energy dispersive X-ray spectroscopy (EDX) analyses were performed with probe currents of approximately 200 pA and collected with an Oxford Instruments X-Max Silicon Drift Detector with an area of 100 mm². The microstructural characterization was correlated to physical and chemical properties by X-ray photoelectron spectroscopy (XPS) at Elettra synchrotron and by cathodoluminescence (CL) in the scanning electron microscope (SEM). A Leica Steroscan SEM and a JEOL 6100 were used for CL measurements. This information is very valuable to unravel the optical properties in oxides. In particular, our results shed some light into the luminescence bands of tin oxide affected by size-effects.

Figure 1(a) shows a general view of a representative SK structure in the SEM. This architecture consists of a Ga-containing trunk, with thicknesses between 50 – 150 nm for different skewers, surrounded by Sn-containing **rhombohedral-shaped** particles as revealed by EDX (inset Figure 1a). The source materials, pure Ga and tin oxide powders, were placed on the top of a gallium oxide pellet, that acted as well as substrate, into an open tubular furnace. Skewer-like structures were extensively produced after 15 h of thermal treatment under an argon gas flux of 0.8 l/min. A video composed by images taken at different times during growth is shown in the *Supplementary Information Video S1*.

To determine the crystallographic relationship between trunk and nanoparticles, TEM analysis was carried out in the as-grown structures. Figure 2(a) shows a low magnification bright field TEM image of a skewer-like structure. Notice the presence of moiré fringes in the superposition of Sn-containing **rhomboidal** particles and the Ga-containing trunk. The moiré fringes indicate an epitaxial relationship between both components, but with different lattice parameter and/or orientation. **In particular, the observed translational moiré fringes (d_{tm}) in the SK structures arises**

from the slight misfit between Ga₂O₃ (110) planes (d_1) and SnO₂ (001) planes (d_2). This misfit could lead to some strain in the SnO₂ particles developed over the Ga₂O₃ wire. Figure S2 (*Supplem. Info*) provides a TEM image of the trunk-particle junction between SnO₂ and Ga₂O₃ and its corresponding FFT pattern. The analysis of the translational moiré pattern observed gives a value of 4.07 nm. On the other hand, the theoretical expected value for the above-mentioned planes is 4.1 nm, which is quite close to the measured periodicity. This result suggests that although a certain degree of strain could be expected from the lattice mismatch, this would occur if just a few layers of SnO₂ were grown over the Ga₂O₃. High-resolution TEM images were recorded in the trunk and the ~~rhombohedral~~ particles (figure 2 (b) and (c) respectively) and the Fourier transform (FT) enabled to identify the β -Ga₂O₃ phase and rutile SnO₂ for the trunk and nanoparticles, respectively. The Ga₂O₃ trunks grow along [110] and surface planes of the Ga₂O₃ NW are the (002) and the (1-10) planes. On the other hand, the SnO₂ particle attached to the NW exhibit facets of {101} type truncated by (200) planes. In Figure S3 (*Supplem. Info*) a ball and stick model is shown that illustrates the lattice matching between (200) planes in SnO₂ and (002) planes of Ga₂O₃. The b lattice parameter of Ga₂O₃ is 3.04 Å while the c parameter of SnO₂ is 3.18 Å.

From these observations, the following formation mechanism of the SK structures is suggested. In the framework of a vapor-solid (VS) mechanism, the first condensed oxide molecules serve as nucleation sites, in a self-catalytic scheme, where further deposition takes place leading to the formation of nanowires if there is a preferred growth direction³⁰. In such a case, the minimization of free energy determines the directional growth during the condensation process, which is dominated by the surface energy growth of nanowires. This can be of crucial importance when it comes to anisotropic materials, as it is the case of the monoclinic β -Ga₂O₃ along the b direction³¹. Previous works have reported Ga₂O₃ NWs with several growth directions [010], [001], [110] or

[40-1] obtained by different methods, such as chemical vapor deposition or thermal deposition and usually in all these works a foreign metal catalyst has been used³²⁻³³. In the present work, Ga₂O₃ NWs are first formed by oxidation of the metallic Ga precursor under dynamical thermal conditions in the furnace. The growth conditions promotes the [110] growth direction for the Ga₂O₃ NWs. This orientation seems to be preferred in thin nanowires. The occurrence of a particular growth direction will give rise to a characteristic faceting of the final nanostructure, which is a key factor when it comes to the formation of more complex nanostructures. Here, the surface facets of the thin NWs favors an epitaxial growth of SnO₂ nanoparticles along the NW with crystalline orientation matching with the Ga₂O₃ axis. The nucleation of these particles could be the out-diffusion of Sn impurities in the Ga₂O₃ NWs. As TEM results show, the surface facets of SnO₂ crystallites are {101} and {200} planes, which is in agreement with a minimization of surface energy in SnO₂³⁴. On the other hand, Sn impurities could be eventually incorporated as well as dopant elements into the Ga₂O₃ NWs, as discussed below. These SK heterostructures reminds the Ge nanoparticles on Si nanowire heterostructures reported in Refs. 10-11, where the proposed driven mechanism was a Plateau-Rayleigh (P-R) instability of the Ge shell around the Si nanowires to reduce the overall surface energy^{10,11}. In addition, the strain due the Si/Ge lattice mismatch was also suggested as an additional factor to modulate the final morphology of the heterostructures¹¹. A strain-mediated growth has also been proposed in the long range ordering of SiGe quantum dots on Si membranes³⁵. In all those cases, the lattice mismatch were significant. We have shown that the [110] oriented Ga₂O₃ nanowires act as a lattice-matching “substrate” for the SnO₂ particles. On the other hand, a clear periodicity of SnO₂ particles around the NWs is not observed in our SKS, but the thickness of these particles seems to be homogeneous along the NW.

This is in agreement with the P-R model where the diameter of the shell is determined by the time duration of the thermal treatment¹⁰.

The addition of chromium impurities in the precursors resulted into Ga₂O₃/SnO₂ CW growth. We have recently reported this architecture²⁶ and made a characterization just at the junction point by means of X-ray absorption near edge structure (XANES) and Extended X-Ray Fine Absorption Structure (EXAFS) analysis. The Cr concentration was found to be 0.014 ± 0.004 atom % Cr in Ga₂O₃, trunk and below the detection limit in SnO₂ wires²⁶. Here, we present the structural characterization performed by HRTEM. From side-view SEM images and EDX compositional analysis of these crossing NWs (Figures 1b and 1c, respectively) straight Ga₂O₃ NW and SnO₂ branches cutting across are easily revealed. The thickness of the Ga₂O₃ NW is of about 250 nm and its length of several microns.

A focused ion beam (FIB) section, perpendicular to the Ga₂O₃ NW growth direction and containing a SnO₂ branch, was fabricated to elucidate the microstructure of the Ga₂O₃/SnO₂ heterojunction (see figure 3(a)). Figure 3(b) (middle) corresponds to the annular dark field (ADF) image with EDX elemental map superimposed (*Ga* in red and *Sn* in green) revealing the Ga₂O₃ NW and the SnO₂ branch in the FIB specimen. High magnification ADF imaging taken in both SnO₂ and Ga₂O₃ (left and right panels, respectively) corresponds to the atomic structure along the [10-1] and [001], respectively. Therefore, the growth direction of the Ga₂O₃ wire has been identified as the [001] direction (along the electron beam) while the crossing SnO₂ wire grows perpendicularly to the Ga₂O₃ wire following the [-101] direction. This result reveals the different Ga₂O₃ growth direction in the SK with respect to the CW structures. The Ga₂O₃ growth direction is [110] in the former and [001] in the latter. Figure 3(c) shows an atomically resolved ADF image of the heterojunction projected onto the (001) and (10-1) planes of Ga₂O₃ and SnO₂ respectively

in the CW structures. Figure 3(d) shows the Fourier Transform of Figure 3(c). Since there are two ordered lattices in the STEM image, there are two set of diffraction spots coming from both lattices. Diffraction spots associated to SnO₂ have been indexed in green and those corresponding to Ga₂O₃ are indexed in red. As it can be seen in the figure, some of these spots overlap. This overlapping reflects lattice coincidence between {310} planes in Ga₂O₃ and {020} planes in SnO₂. The image shows that both nanowires are joined by an interface boundary, which is not edge-on under these TEM conditions.

The structural analysis of the Ga₂O₃/SnO₂ CWs would help to get some insight into their formation. If we assume that the first step is the growth of the Ga₂O₃ NWs, we have to elucidate the reason for the growth of either SnO₂ nanowires across them or SnO₂ nanoparticles attached to them (shown above). The mechanism seems to be related to the particular growth direction of the Ga₂O₃ axis, with the implications of this fact on the surface energy of the NWs facets. The obtained growth direction is [110] for NWs in SK nanostructures and [001] for NWs in the crossing Ga₂O₃/SnO₂ structures. The thermal treatments and source materials in both treatments were similar, except for the presence of chromium oxide in case of crossing structures. In H. J. Chun's *et al.* study of Ga₂O₃ NW growth, it was found that the structure of the NW could be controlled with the use or not of the metal catalyst, and that the nanowires grown with nickel as catalyst have random growth direction³². Here, the addition of a small amount of chromium into the source materials could have influenced the mobility and diffusion of the adsorbed species in the Ga₂O₃ primary NWs leading to [001] NWs instead of [110] ones when only gallium and tin were present. Moreover, a specific growth direction involves specific lateral surface planes of the NW, which implies that surface energy engineering could be used to control the final morphology of the nanostructures. It should be taken into account that we use a VS mechanism, with no external

catalyst. Crossing InSb nanowires have been obtained by a vapor-liquid-solid (VLS) method, which use gold as catalyst, in a four-step process³⁶. An example of combined nucleation and surface energy engineering to get tuned structures has been recently published in III-V nanowires¹², where the provoked effect was the kinks formation in the GaAs NWs by modifying growth conditions. In this work, SnO₂ nanostructures are able to grow during the same thermal process. We have observed that the primary Ga₂O₃ wire orientation could serve as an engineering tool to get different architectures: i) the growth of SnO₂ particles decorating the main thin Ga₂O₃ axis, leading to the skewers; or ii) the growth of SnO₂ cross wires across the Ga₂O₃ wires.

In order to assess local optical and chemical properties of these complex morphologies, spatially resolved XPS and CL measurements have been carried out. CL in the SEM enables to probe electronic levels across the whole nanostructure (penetration depth of electron beam in the SEM is slightly lower than 1 μm , for $V_{\text{acc}} = 15 \text{ kV}$) while XPS measurements provides information about the electronic states and chemical bonding at the surface level.

XPS analysis with high spatial resolution has been performed at the ESCA microscopy line at Elettra synchrotron in Trieste. The operation conditions at this beamline balance quite well the trade-off between spatial and energy resolution. XPS spectra were performed with 648 eV photon energy. This means that kinetic energy of electrons is around 100 - 600 eV. Therefore, the mean free path (probe depth for XPS signal) is $\approx 10 \text{ \AA}$. Hence, surface effects strongly influence the information on electronic properties. High-resolution XPS spectra were recorded to get the energy profiles of Ga 3d, Sn 4d, Sn 3d and O 1s core levels, which gives information about the chemical bonding. Energy axis in high resolution spectra was calibrated by fixing the C 1s binding energy (BE) at 248.8 eV³⁷. Figure 4 summarizes the XPS results from the SK and CW architectures. Figure 4 (center) shows XPS maps representing the intensity of the Ga 3d line of both structures.

High-resolution spectra from the central Ga₂O₃ axis in skewer-like structures and in cross wires are shown in Figure 4 (left - points marked as “a” in the XPS images). The binding energies for Ga 3d and Sn 4d core levels are 20.5 eV and 26.0 eV, respectively. We have selected this window energy because we can simultaneously obtain information about both elements in the same experiment. The results show the main Ga 3d peak in the axis of both nanostructures, but in the SK structures, a non-negligible peak is observed at 26 eV that corresponds to the Sn 4d binding energy level. The Ga 3d binding energy of 20.5 eV corresponds to the Ga³⁺ in the Ga – O bonding, in undoped material³⁸. A slight shift towards higher energies is observed in the XPS spectrum of point a, in the skewer axis (Figure 4 (left)). This would be consistent with the presence of Sn in the skewer axis as dopant, but not in the axis of CWs. Alternatively, spectra from the SnO₂ particles and SnO₂ cross wires have also been obtained from XPS maps (points marked as “b”) and displayed at the right in Figure 4 (right). The dominant peak corresponds to the Sn 4d line, but it is worth noticing that the Ga 3d line is rather important in both SnO₂ particles and nanowires. This result shows that both nanowires and nanoparticles are Ga doped, at least at the surface level. XPS spectra of the Sn 3d_{5/2} and O 1s lines have also been recorded (Figure S4 in the *supplementary info*). The XPS analysis has also revealed a small peak at 487 eV (Sn 3d_{5/2} level) in the Ga₂O₃ axis of the SKs and changes in the line profile of the O 1s levels. Hence, these XPS results suggest that the Ga₂O₃ nanowire axis in the SKs are slightly Sn doped while the axis in CWs seem to be undoped.

Finally, we have investigated the luminescence of both kinds of nanostructures, SK and CW, by means of CL. The high spatial resolution of the CL technique enables to get local CL spectra at different points in the structures. Since the quantum efficiency of both Ga₂O₃ and SnO₂ is rather high, all the CL measurements have been carried out at room temperature. Even though

semiconductor oxides exhibit a wide bandgap, visible luminescence occurs quite often due to the presence of oxygen vacancies that give rise to luminescence centres. In many cases, the oxygen vacancies may form complex defects with other point defects or impurities, which makes the visible luminescence bands rather broad.

Figure 5a shows the secondary electron image of a SK structure where “A” label stands for axis and “B” label for particles. Figure 5b shows the spectra acquired at the Ga₂O₃ axis and at the tip of one of the SnO₂ particles attached to the main NW in the SK structures. The CL emission from Ga₂O₃ corresponds to the ultraviolet (UV) band composed of two components (3.3 and 3.0 eV) related to bound excitons and donor-acceptor pair with (DAP) transitions³⁹. Both donor and acceptor centers involve native point defects, with the oxygen vacancy V_O generally accepted to act as the donor center, while V_{Ga}-V_O complexes are considered to be acceptors⁴⁰. This emission is characteristic of undoped Ga₂O₃. CL spectra of pellets of Ga₂O₃ and SnO₂ oxides, which have been used as reference samples, with their usual native-defects related UV and visible bands, respectively, are displayed in the Figure S5 (*suppl. info*). It can be seen that the CL spectrum from the axis wire (spectrum A) is quite similar to that shown in Figure S5. On the other hand, known luminescence bands in SnO₂ are the orange (OR) band at 1.95 eV (635 nm), related to oxygen vacancies, and a green – blue (GB) band, which is strongly dependent on surface states⁴¹. Several GB bands at 2.25 and 2.58 eV (550 and 480 nm) have been reported in SnO₂ microcrystals, with relative intensities dependent on surface facets and thermal treatments⁴². In our case, the CL emission of the SnO₂ particles exhibits the GB band and blue emission composed of several bands (2.76 and 2.95 eV), which is unusual. No significant orange emission is found in the SnO₂ particles. Similar blue-UV emission has been reported in SnO₂ nanoparticles and attributed to quantum confinement effects⁴³, which can be ruled out here since the SnO₂ particles in the skewer structures

are around 800-900 nm. However, the particles display well-defined facets that may have characteristic surface states⁴¹. This could explain the observed blue-UV emission and the quenching of the orange band.

A CL analysis of the crossed Ga₂O₃-SnO₂ wires is summarized in Figures 5(c-f). Figure 5(c) shows the secondary electron image of a CW assembly. CL emission from Ga₂O₃ axis shows the characteristic UV band but also a not negligible broad band in the orange region (Figure 5d). On the other hand, the orange band (1.95 eV) dominates the CL spectrum from the SnO₂ wires. As it has been mentioned, this OR band is commonly attributed to oxygen vacancies in SnO₂ bulk material⁴⁴. Therefore, the CL emission from the SnO₂ wires crossing the Ga₂O₃ axis is dominated by native defects instead of surface states, in contrast to the emission of SnO₂ particles in the skewer like structures, where the main CL bands are those of the blue-UV region. These results agree with the above-described structural and surface analysis. Monochromatic CL images of the characteristic emission bands of both Ga₂O₃ axis and SnO₂ wires are displayed in Figures 5(e) and 5(f). The main ultraviolet emission comes from the central trunk, while crossing wires are emitting orange light. In addition, the orange light that arises in the main Ga₂O₃ axis could come from waveguiding luminescence of the SnO₂ cross wires. The luminescence results demonstrate a dependence on the shape of the luminescence properties in the case of SnO₂. Therefore, shape engineering could be a useful approach to capitalize the plenty of possibilities of semiconductor oxides assemblies.

In summary, the Ga₂O₃-SnO₂ material system has been revealed as a platform to study orientation dependent architectures and properties. A thermal evaporation method at high temperature, close to the melting points of both oxides, allows the formation of either skewer-like (SK) structures or crossed wires (CW). The root of these architectures is a primary Ga₂O₃ nanowire

with a preferred growth direction. In the SK structures, Sn out-diffusion in the [110] Ga₂O₃ NWs may nucleate the formation of SnO₂ particles further developed with a nice lattice matching between the surface axis and the particles. The observed facets in the SnO₂ particles are compatible with minimum surface energy considerations. On the other hand, the addition of a small amount of chromium oxide in the source materials leads to the formation of crossed Ga₂O₃-SnO₂ wires. In this case, the growth direction of the Ga₂O₃ nanowires is the [001], probably induced by the presence of chromium. In this scenario, Sn impurities in the main Ga₂O₃ axis seem to act as nucleation sites for SnO₂ wires at some points of the main axis in a secondary growth self-catalyzed scheme. The Ga₂O₃/SnO₂ junction in CW structures examined by HRTEM has been revealed as a grain boundary and it seems that the lattice matching condition is not required for the formation of the CW structures. XPS results demonstrate the presence of a small amount of Sn in the main Ga₂O₃ axis of skewer structures, not observed in the Ga₂O₃ axis of the crossing wires. On the other hand, CL emission of SnO₂ has been shown to be affected by its shape and dimensions of the structures. Both assemblies show luminescence at room temperature. While CL of SnO₂ wires in the cross structures is dominated by the orange band, the CL emission of SnO₂ particles is dominated by blue emission probably originated by the exposure of specific surface facets with characteristic surface states.

FIGURES

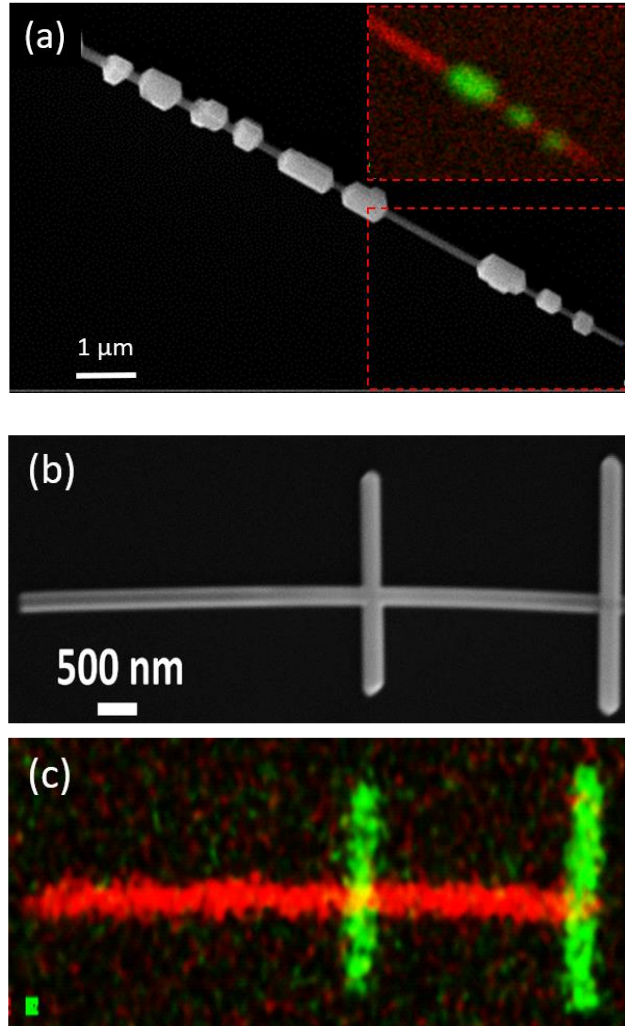


Figure 1. (a) SEM image of a skewer-like structure. Inset: the corresponding EDX map for Ga and Sn elements of the red square. Source materials were Ga chips and SnO₂ powders and the thermal treatment was carried out at 1500 °C for 15 hours. (b) SEM image of several SnO₂ wires crossing a main Ga₂O₃ nanowire obtained after the addition of a small fraction of chromium oxide to the precursors and follow the same thermal treatment as in (a), and (c) its corresponding EDX mapping of Sn (green) and Ga (red) elements.

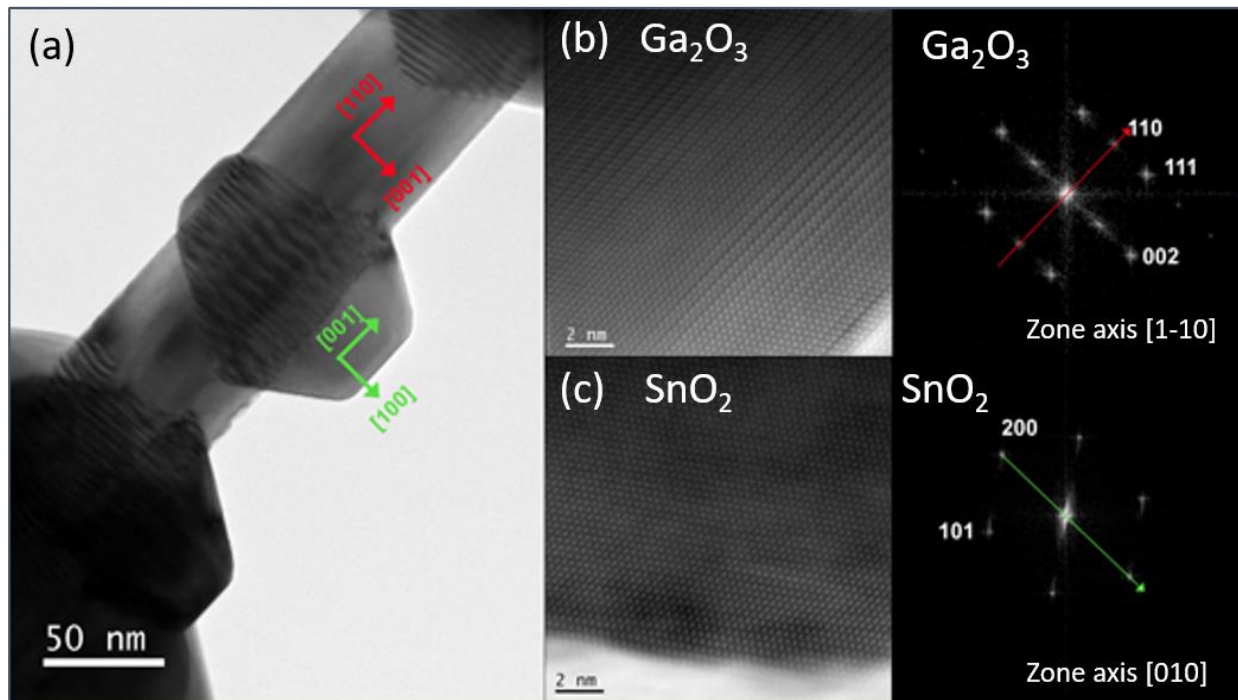


Figure 2. (a) TEM image of skewer-like structure. (b) HRTEM analysis of the Ga_2O_3 main axis of a skewer-like structure and its corresponding Fourier Transform (FT) pattern. (c) HRTEM image of the SnO_2 particle and its FT pattern.

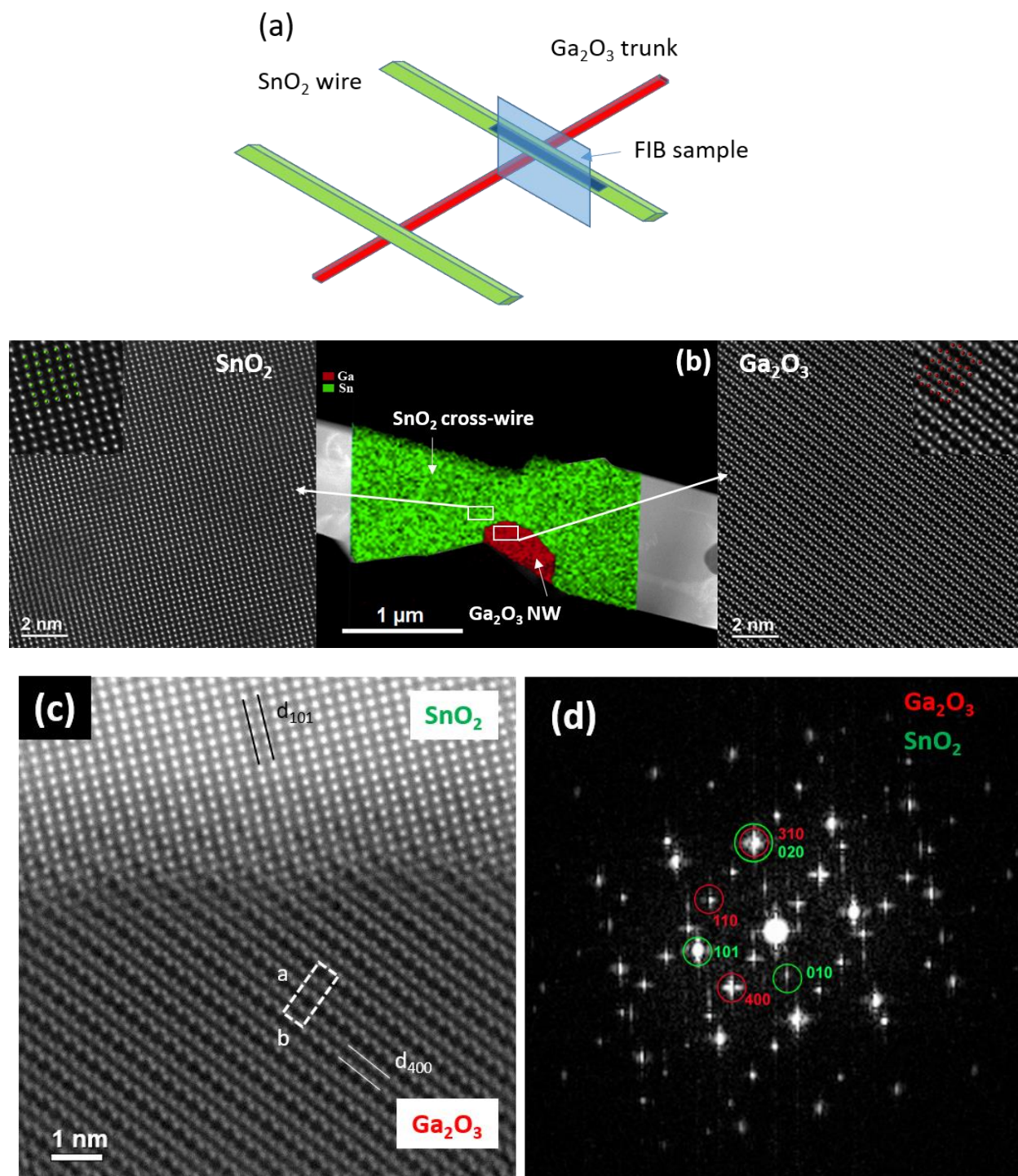


Figure 3. (a) Artwork depicting the cross-section of the junction area between SnO₂ and Ga₂O₃ nanowires prepared by Focused Ion Beam technique. (b) TEM analysis of the cross-section area of crossing wires prepared by FIB (central image) overlapped with the compositional

information provided by EDX (Ga in red, Sn in green). Left: high resolution STEM of SnO₂ wire. Right: high resolution STEM of the central Ga₂O₃ wire. Both STEM images have been acquired at the regions marked with a white square in (b). Insets display atom resolution ADF images overlapped with ball model crystal structures in both cases. Oxygen atoms are hidden in the balls model. (c) Atomically resolved ADF image of the heterojunction projected onto the (001) and (10-1) planes of Ga₂O₃ and SnO₂ respectively in the crossing wires structures. The projection of the Ga₂O₃ unit cell is drawn. (400) planes in Ga₂O₃ and (101) planes in SnO₂ are also marked. (d) Fast Fourier Transform (FFT) of (b) that reveals lattice coincidence between {310} planes in Ga₂O₃ and {020} in SnO₂.

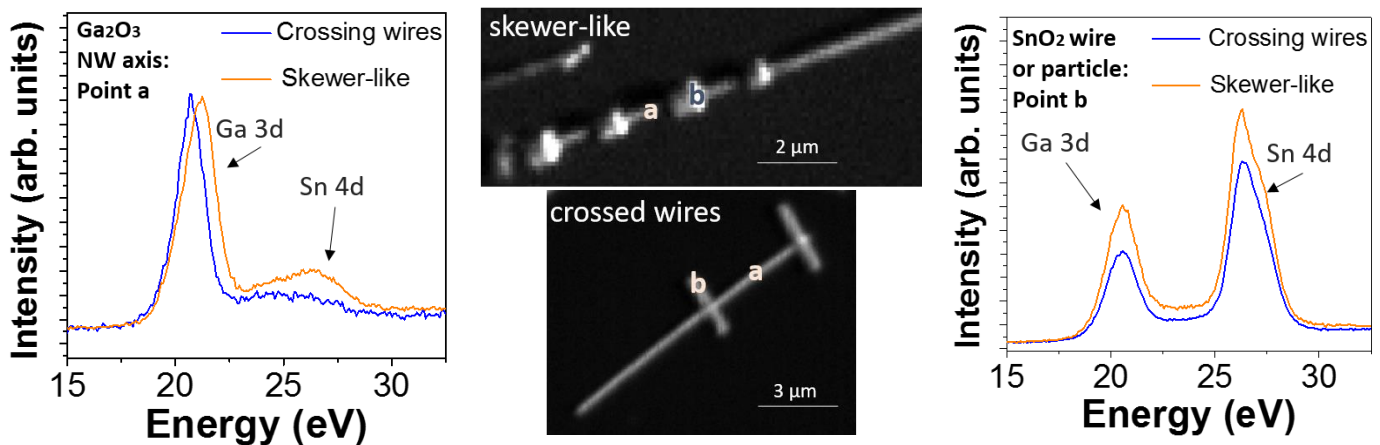


Figure 4. Left: XPS spectra obtained from the main Ga₂O₃ nanowire axis in crossing wires (blue line) and skewer-like structures (red line). Center: XPS Ga 3d map of both structures. Right: XPS spectra recorded at SnO₂ crossing wires (blue line) and at SnO₂ particles (red line).

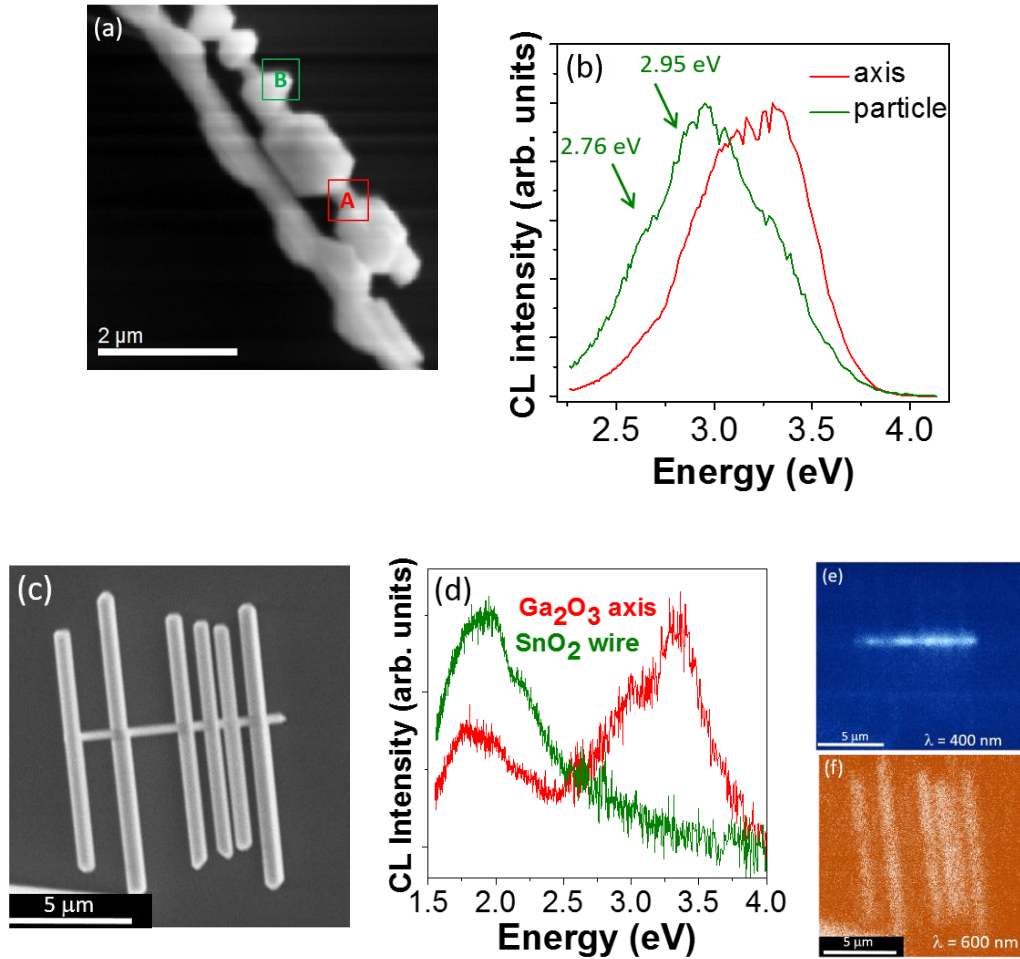


Figure 5. (a) Secondary electron image of SK structures. (b) CL spectra recorded at the points labelled as A and B in (b) corresponding to the Ga₂O₃ nanowire axis and the SnO₂ particle, respectively. (c) Secondary electron image of a CW structure. (d) CL spectra from Ga₂O₃ axis and one of the SnO₂ branches. (e) monochromatic CL image at $\lambda = 400$ nm, and (f) monochromatic CL image at $\lambda = 600$ nm of the CW structure shown in (c).

ASSOCIATED CONTENT

Supporting Information

In-situ video growth of Ga₂O₃/SnO₂ nanostructures (gif) and additional figures (pdf).

AUTHOR INFORMATION

Corresponding Authors

*E-mail: a.m.sanchez@warwick.ac.uk , bianchi@ucm.es

Author Contributions

The manuscript was written through contributions of all authors. All authors have given approval to the final version of the manuscript.

Notes

The authors declare no competing financial interest.

ACKNOWLEDGMENTS

This work has been supported MINECO (projects CSD 2009-00013, MAT 2012--31959, MAT 2015-65274-R-FEDER). We thank Richard Beanland for his advice at Warwick University. We also thank Luca Gregoratti for his assistance at ESCA microscopy beamline at Elettra Sincrotrone. Bianchi Méndez acknowledges the mobility Grant supported by MEC (PRX14/00134) for sabbatical leave at Warwick University.

REFERENCES

1. Li, C.; Yu, Y.; Chi, M.; Cao, L. *Nano Lett.* **2013**, 13, 948–953.
2. Borgström, M. T.; Zwiller, V.; Müller, E.; Imamoglu, A. *Nano Lett.* **2005**, 5, 1439–1443.
3. Liu, Q.; Lu, H.; Shi, Z.; Wu, F.; Guo, J.; Deng, K.; Li, L. *ACS Appl. Mater. Interfaces* **2014**, 6, 17200–17207.
4. Lu, J. G.; Chang, P.; Fan, Z. *Mater. Sci. Eng. R-Rep.* **2006**, 52, 49–91.
5. Wang, Z. L. *Adv. Mater.* **2003**, 15, 432–436.
6. Huang, M. H.; Mao, S.; Feick, H.; Yan, H.; Wu, Y.; Kind, H.; Weber, E.; Russo, R.; Yang P. *Science* **2001**, 292, 1897–1899.
7. Lieber, C.M.; Wang, Z.L. *MRS Bulletin* **2007**, 32, 99-108.
8. Sirbuly, D. J.; Tao, A.; Law, M.; Fan, R.; Yang, P. *Adv. Mater.* **2007**, 19, 61–66.
9. Varley, J. B.; Janotti, A.; Franchini, C.; Van de Walle, C. G. *Phys. Rev. B* **2012**, 85, 081109.
10. Day, R. W.; Mankin, M. N.; Gao, R.; No, Y.-S.; Kim, S.-K.; Bell, D. C.; Park, H.-G.; Lieber, C. M. *Nat. Nanotechnol.* **2015**, 10, 345– 352.
11. Day, R. W.; Mankin, M.N.; Lieber, C. M. *Nano Lett.*, **2016**, 16, 2830-2836.
12. Yuan, X.; Caroff, P.; Wong-Leung, J.; Fu, L.; Tan, H. H.; Jagadish, C.; *Adv. Mater.* **2015**, 27, 6096–6103.
13. Ly, C.; Peng, Z.; Zhao, Y.; Huang, Z.; Zhang, C J. *Mater. Chem. A* **2016**, 4, 1454-1460.
14. Hou, J.; Qu, Y.; Krsmanovic, D.; Ducati, C.; Eder, D.; Kumar, R. V. *J.Mater.Chem.* **2010**, 20, 2418–2423.
15. Cheng, J. J.; Nicaise, S. M.; Berggren, K. K.; Gradecak, S. *Nano Lett.* **2016**, 16, 753–759.
16. Hidalgo, P.; Méndez, B.; Piqueras, J. *Nanotechnol.* **2005**, 16, 2521-2524.
17. Díaz-Guerra, C.; Piqueras J. *Cryst. Growth Des.* **2008**, 8, 1031-1034.

18. Alemán, B.; Fernández, P.; Piqueras, J. *Appl. Phys. Lett.* **2009**, 95, 013111.
19. Maestre, D.; Häussler, D.; Cremades, A.; Jäger, W.; Piqueras, J. *Jour. Phys. Chem. C* **2011**, 115, 11083.
20. Jin, S.; Wang, X.; Wang, X.; Ju, M.; Shen, S.; Liang, W.; Zhao, Y.; Feng, Z.; Playford, Y. L.; Walton, R. I.; Li, C. *J. Phys. Chem. C* **2015**, 119, 18221–18228.
21. López, I.; Castaldini, A.; Cavallini, A.; Nogales, E.; Méndez, B.; Piqueras, J. *J. Phys D: Appl. Phys.* **2014**, 47, 415101.
22. Martinez, C. J.; Hockey, B.; Montgomery, C.B.; Semancik, S. *Langmuir* **2005**, 21, 7937–7944.
23. Abd-Ellah, M.; Bazargan, S.; Thomas, J. P.; Rahman, M. A.; Srivastava, S.; Wang, X.; Heining, N. F.; Leung, K. T. *Adv. Electron. Mater.* **2015**, 1, 1500032.
24. Mazeina, L.; Picard, Y. N.; Maximenko, S. I.; Perkins, F. K.; Glaser, E. R.; Twigg, M. E.; Freitas, J.A.; Prokes, S. *Cryst. Growth Des.* **2009**, 9, 4471–4479.
25. Hsu, C. L.; Lu, Y. C. *Nanoscale* **2012**, 4, 5710.
26. Martínez-Criado, G.; Segura-Ruiz, J.; Chu, M. H.; Tucoulou, R.; López, I.; Nogales, E.; Méndez, B.; Piqueras, J. *Nano Lett.* 14, 5479–5487.
27. Hidalgo, P.; Méndez, B.; Piqueras, J. *Nanotechnol.* **2008**, 19, 455705.
28. Cebriano, T.; Ortega, Y.; Hidalgo, P.; Maestre, D.; Méndez, B.; Piqueras, J. *Nanotechnol.* **2014**, 25, 235701.
29. López, I.; Nogales, E.; Méndez, B.; Piqueras, J.; Peche, A.; Ramirez-Castellanos, J.; González-Calbet, J. *J. Phys. Chem. C* **2013**, 117, 3036–3045.
30. Lu, J. G.; Chang, P.; Fan, Z.; *Materials Science and Engineering R* **2006**, 49-91.
31. Ueda, N.; Hosono, H.; Waseda, R.; Kawazoe, H. *Appl. Phys. Lett.* **1997**, 71, 933.

32. Chun, H. J.; Choi, Y. S.; Bae, S. Y.; Seo, H. W.; Hong, S. J.; Park, J.; Yang, H. *J. Phys. Chem. B* **2003**, 107, 9042–9046.
33. Hosein, I. D.; Hegde, M.; Jones, P. D.; Chirmanov, V.; Radovanovic, P. V. *J. Cryst. Growth* **2014**, 396, 24–32.
34. Batzill, M.; Diebold, U. *Prog. Surf. Sci.* **2005**, 79, 47–154.
35. Ritz, C. S.; Kim-Lee, H.-J.; Detert, D. M.; Kelly, M. M.; Flack, F.; Savage, D. E.; Cai, Z.; Evans, P. G.; Turner, K. T.; Lagally, M. G. *New J. Phys.* **2010**, 12, 103011.
36. Plissard, S. R.; van Weperen, I.; Car, D.; Verheijen, M. A.; Immink, G. W. G.; Kammhuber, J.; Cornelissen, L. J.; Szombati, D. B.; Geresdi, A.; Frolov, S. M.; Kouwenhoven, L. P.; Bakkers, E. P. A. M. *Nat. Nanotechnol.* **2013**, 8, 859–864.
37. Miller, D. J.; Biesinger, M. C.; McIntyre, N. S. *Surf. Interface Anal.* **2002**, 33, 299.
38. López, I.; Utrilla, A.; Nogales, E.; Méndez, B.; Piqueras, J.; Peche, A.; Ramirez-Castellanos, J.; González-Calbet, J. *J. Phys. Chem. C* **2012**, 116, 3935.
39. Binet, L.; Gourier, D. *J. Phys. Chem. Solids* **1998**, 59, 1241–1249.
40. Shimamura, K.; Villora, E. G.; Ujiie, T.; Aoki, K. *Appl. Phys. Lett.* **2008**, 92, 201914.
41. Yuan, X. L.; Lazzarini, L.; Salviati, G.; Zha, M.; Sekiguchi, T. *Mat. Sci. Semicond. Process.* **2006**, 9, 331–336.
42. Maestre, D.; Cremades, A.; Piqueras, J. *J. Appl. Phys.* **2005**, 97, 044316.
43. Das, S.; Kar, S.; Chaudhuri, S. *J. Appl. Phys.* **2006**, 99, 114303.
44. Maestre, D.; Cremades, A.; Piqueras, J. *J. Appl. Phys.* **2004**, 95, 3027.

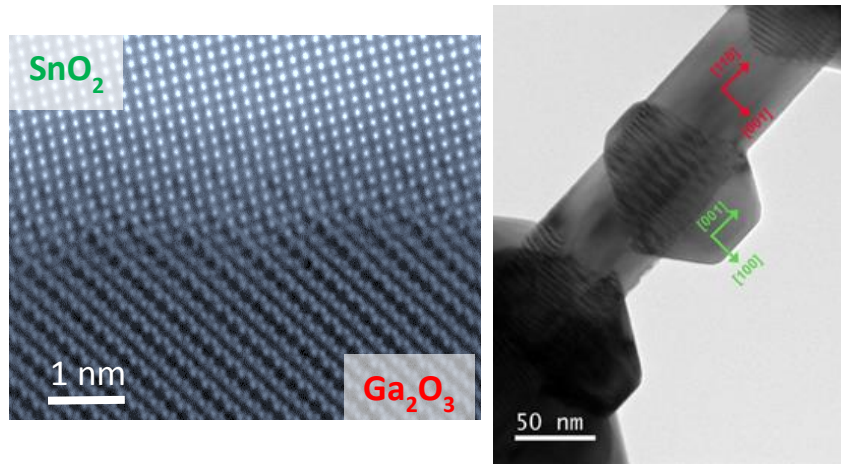


Table of Contents Graphic